

Structural evolution and controls on gold mineralization at Clear Creek, Yukon

J.R. Stephens, N.H.S. Oliver and T. Baker

James Cook University¹

C.J.R. Hart²

Yukon Geology Program

Stephens, J.R., Oliver, N.H.S., Baker, T. and Hart, C.J.R., 2000. Structural evolution and controls on gold mineralization at Clear Creek, Yukon. *In: Yukon Exploration and Geology 1999*, D.S. Emond and L.H. Weston (eds.), Exploration and Geological Services Division, Yukon, Indian and Northern Affairs Canada, p. 151-163.

ABSTRACT

Gold mineralization in the Clear Creek area is associated with ca. 92 Ma Tombstone Plutonic Suite intrusions (TPS) emplaced into metasedimentary rocks of the Neoproterozoic to Early Cambrian Hyland Group. Hyland Group rocks have undergone four ductile deformations (D_1 - D_4) in the structurally thick (>10 km) Jura-Cretaceous Tombstone high strain zone. Kinematic features indicate overall top-to-the-northwest movement on shallow shear planes. Four different types of quartz veins developed during ductile deformation and are associated with a progression from ductile to brittle-ductile behaviour. Three major brittle structural trends postdate ductile deformation. A set of sinistral $\sim 165^\circ$ striking faults developed and are crosscut by secondary east-west fracture zones in Hyland Group rocks. The Tombstone Plutonic Suite was then emplaced in a broadly east-west oriented belt, with some local control exerted by the $\sim 165^\circ$ oriented faults. Continued development of the east-west fracture set after the Tombstone Plutonic Suite intrusion, resulted in an extensive system of gold-bearing sheeted quartz veins. Finally, sinistral reactivation and associated quartz-tourmaline veining occurred on $\sim 165^\circ$ oriented structures.

Preliminary analysis of fault geometry and connectivity suggests the most favourable sites for mineralization are east-west fracture zones connected to $\sim 165^\circ$ oriented faults. Other favourable structural sites include misoriented segments of $\sim 165^\circ$ faults and possibly northeast-striking structures connected to $\sim 165^\circ$ faults. Mapping has delineated a large area of contact metamorphism suggesting extensive shallowly buried intrusions. The highest priority in any exploration program should be given to sites that are coincident with shallowly buried, or that are near Tombstone Plutonic Suite intrusions and have the above fault/fracture geometries.

RÉSUMÉ

La minéralisation aurifère dans la région de Clear Creek est associée à des intrusions de la Suite plutonique de Tombstone (SPT), datant de 92 Ma, qui ont été mises en place dans les roches métasédimentaires du Groupe de Hyland du Protérozoïque tardif au Cambrien précoce. Dans la zone structurellement épaisse (>10 km) intensément déformée de Tombstone (d'âge Jura-Crétacé) les roches du Groupe de Hyland ont subi quatre épisodes de déformation ductile (D_1 à D_4). Les indicateurs cinématiques témoignent de mouvements le long de plans de cisaillement à pendage faible à vergence vers le nord-ouest. Quatre types différents de veines de quartz ont été formés lors de la déformation ductile et sont associés au changement de caractère du mouvement de ductile à ductile-cassant. Trois axes structuraux principaux à caractère cassant ont suivi la déformation ductile. Un jeu de failles de direction $\sim 165^\circ$ et à mouvement senestre a été formé dans les roches du Groupe Hyland et a été suivi par la formation de zones de fractures secondaires orientées vers l'est. La SPT s'est mise en place le long d'une ceinture orientée grossièrement est-ouest, localement contrôlée par les failles orientées à $\sim 165^\circ$. La continuation du développement du jeu de fractures orientées est-ouest a produit un vaste réseau de filons parallèles de quartz aurifère. Finalement, une réactivation du mouvement senestre a été accompagnée par la formation de veines de quartz-tourmaline dans les structures orientées à $\sim 165^\circ$.

Une analyse préliminaire de la géométrie et de la connectivité des failles indique que les sites les plus favorables pour la minéralisation sont les zones de fractures orientées est-ouest qui interceptent les failles orientées à $\sim 165^\circ$. D'autres sites structuraux favorables incluent les segments des failles à $\sim 165^\circ$ dont l'orientation a été changée ainsi que, peut-être, les structures orientées nord-est qui interceptent les failles à $\sim 165^\circ$. Une vaste étendue de métamorphisme de contact, mise à jour par la cartographie sur le terrain, suggère la présence d'intrusions d'envergure à faible profondeur. On devrait accorder la plus haute priorité aux programmes d'exploration ciblant les sites qui coïncident avec des intrusions à faible profondeur de la SPT ou qui sont situés à leur proximité et qui présentent les géométries de failles et de fractures qui ont été décrites ci-haut.

¹Economic Geology Research Unit, School of Earth Sciences, James Cook University, Townsville, Queensland, 4811, Australia, julian.stephens@jcu.edu.au

²craig.hart@gov.yk.ca

INTRODUCTION

This study was initiated in order to evaluate the structural, environmental, as well as temperature and pressure conditions, associated with emplacement of Tombstone Plutonic Suite (TPS) intrusions and related gold mineralization. The focus of 1999 field work was the Clear Creek area, with the initial goals as follows:

- Establish the structural setting of granite emplacement.
- Determine the structural and thermal history of the area.
- Place the formation of gold-bearing veins into a paragenetic framework.

The main methods used in this study were field mapping and structural analysis.

LOCAL GEOLOGY

The Clear Creek area is underlain by (in order of abundance) psammite, phyllite, quartzite, conglomerate, schist and calc-silicate rocks of the Neoproterozoic to Early Cambrian Hyland Group (Fig. 1). These rocks have been deformed and metamorphosed in the structurally thick (>10 km) Jura-Cretaceous Tombstone high-strain zone 'THSZ' (Tombstone Strain Zone of Murphy, 1997). Multiple deformation events indicate overall top-to-the-northwest movement on shallow north-dipping planes. These fabrics have been folded by the broad, upright, gently west-plunging McQuesten Antiform.

The TPS intruded deformed Hyland Group rocks under shallow crustal conditions (<3 kb – Baker and Lang, 1999). The intrusions clearly crosscut the main ductile fabrics in the THSZ, and have been dated at 91.4 ± 0.8 Ma (Murphy, 1997). Marsh et al., (1999) described six stocks of the TPS in the Clear Creek area (Fig. 2). The stocks range in composition from medium- to

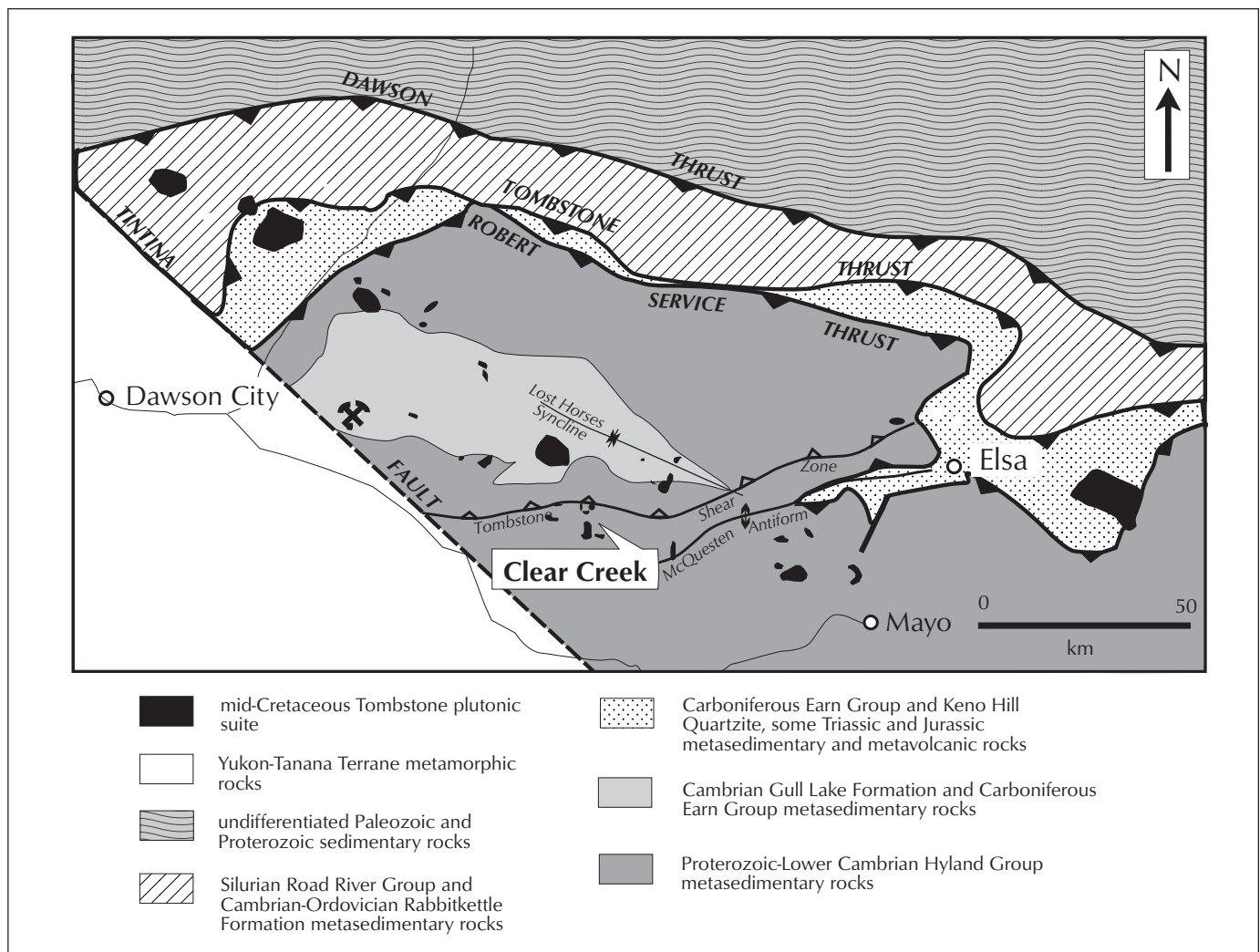


Figure 1. Location and regional geology map (after Murphy, 1997).

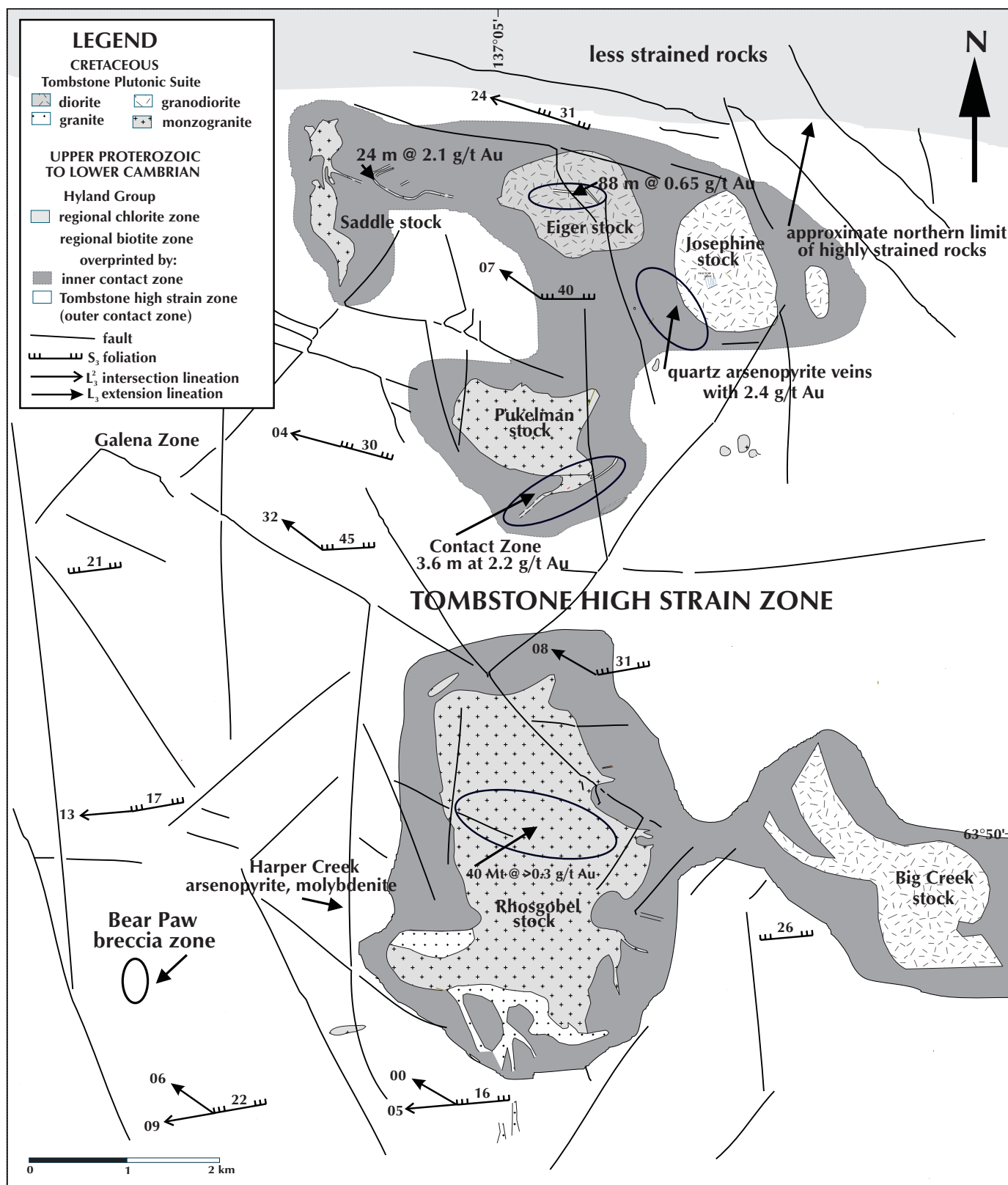


Figure 2. Geological map of the Clear Creek area with metamorphic zones.

coarse-grained quartz monzonite to granodiorite and diorite. There is a broad compositional zoning of the main intrusions at Clear Creek, with more mafic (diorite and granodiorite) plutons to the east and more felsic (quartz monzonite) plutons to the west. West of the main Clear Creek area, however, the Grizzly stock (Allen et al., 1998) and Barney stock have east-west elongation, parallel to the regional trend of the TPS belt. Contact metamorphic aureoles with andalusite and biotite porphyroblasts, and finer grained biotite are present around the stocks. Gold occurs in veins within and surrounding most of these intrusions (Marsh et al., 1999). Recent exploration has outlined significant gold grades over 2 km away from any known, exposed granitoid stocks (Redstar Resources, 1999). Clear Creek has also produced in excess of 130,000 reported ounces of gold (4 million grams).

METAMORPHISM

A two-stage metamorphic evolution has affected sedimentary rocks at Clear Creek. Jura-Cretaceous regional metamorphism was followed by mid-Cretaceous contact metamorphism associated with TPS emplacement. Our mapping, and work by Murphy (1997), indicate that biotite grade was attained during ductile deformation of the THSZ, while the less deformed rocks north of the THSZ only attained chlorite grade. Preliminary petrography indicates peak regional metamorphism in the THSZ occurred during D_2 . Regional metamorphic assemblages are overprinted by contact metamorphism associated with intrusion of the TPS stocks. Broad zones of andalusite and biotite porphyroblasts (Fig. 3) and localized cordierite in pelites occur around the stocks, with garnet present within a few metres of intrusion contacts.

The contact aureoles are divisible into two broad zones (Fig. 2).

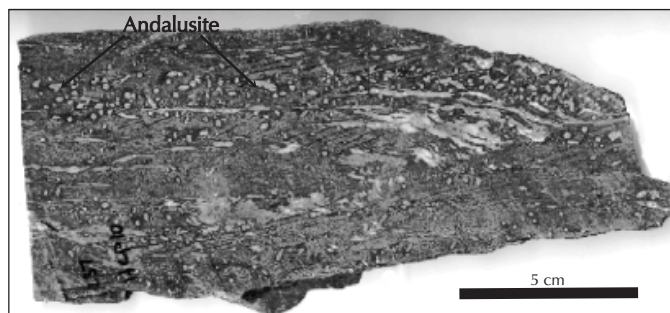


Figure 3. Polydeformed biotite-muscovite schist overprinted by contact metamorphic andalusite porphyroblasts.

- 1) The inner zone is characterized by strongly recrystallized quartz and biotite in pelites and psammities, as well as strong andalusite and local cordierite growth in aluminous rocks. These hornfelsed rocks are strongly resistant, comprise the highest peaks in the area, and extend about 200-500 m laterally from intrusion contacts. The boundary of these zones is marked by a distinct break in slope.
- 2) An outer zone of contact metamorphism was recognized while mapping. It is defined by andalusite and biotite growth in pelitic rocks and extends at least 3 - 5 km from any known plutons. The outer boundary of this zone is poorly defined, but intriguingly, does not appear to extend into rocks north of the THSZ.

Therefore, a larger area of contact metamorphism than previously known is recognized in this study. This is interpreted to represent an extensive system of shallowly buried intrusions in the area.

STRUCTURE

DUCTILE DEFORMATION FEATURES

Murphy (1997) suggested that the THSZ is the palaeo-depth extension of the Tombstone Thrust. Multiple deformation features in the THSZ indicate overall top-to-the-northwest transport (Murphy, 1997) and are confirmed by this work.

Hyland Group rocks in the Clear Creek area have undergone four major ductile deformational events, which are correlated with those defined by Murphy (1997), and Mair (this volume) in Table 1. D_1 produced a poorly preserved spaced cleavage, S_1 (Fig. 4). D_2 produced rarely preserved isoclinal folds, F_2 , with a strong axial planar schistosity, S_2 , which is locally mylonitic. D_3 produced tight, reclined, neutral to south-vergent, well preserved 1-cm to 10-cm-scale F_3 folds, which plunge gently west and have a moderate to strongly developed axial planar foliation, S_3 . A pervasive extension lineation, L_3 , is typically inclined at 35° north of F_3 fold axes (and by definition L_3 intersection lineation) on the S_3 foliation plane, and has a northwest plunge (Fig. 5). Weakly developed open crenulations, $F_{4'}$ were the last small-scale ductile feature to develop. These plunge gently to the northeast and have upright axial planes, with a rarely developed axial planar foliation, S_4 .

A protracted history of quartz vein formation during ductile deformation has been identified (Fig. 6). The first veins to develop during early D_2 are strongly boudinaged and isoclinally folded (DV_a). These were followed by boudin-neck veins during D_3 (DV_b), and then tension veins late in D_3 (DV_c). Paragenetic relationships suggest these three vein types developed progressively throughout early D_2 to late D_3 . Slightly boudinaged, steep quartz veins that strike $\sim 140^\circ$ (DV_d) are the last set to show any ductile deformation features.

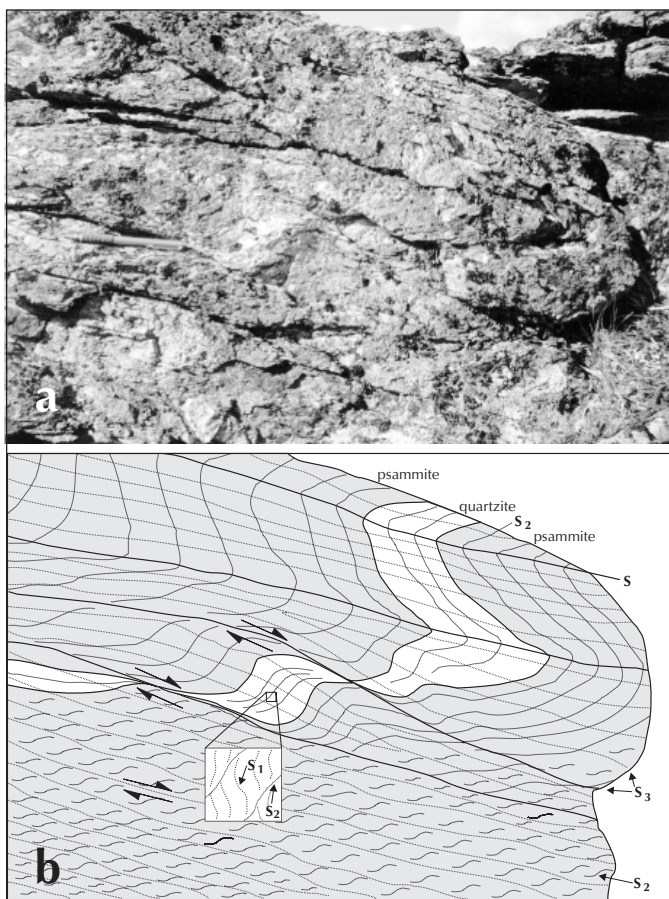


Figure 4. a) F₃ fold of quartzite and psammite layers just west of the Rhosgobel stock, looking west. b) Sketch of outcrop in a) showing the relationship of THSZ fabrics in the area. Note the southerly to neutral vergence of F₃ folds and S₂/S₃ fabric relationships. The top half of the outcrop has undergone less intense deformation during D₃ due to strain partitioning around the hinge of a more competent quartzite layer.

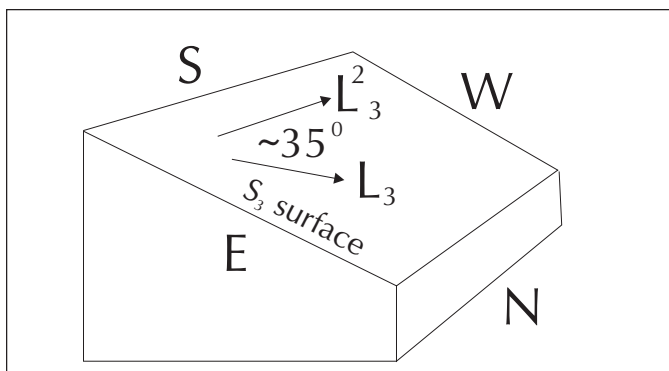


Figure 5. Block diagram showing the consistent angular relationship of the L₃²/F₃ intersection lineation/fold axes to the L₃ extension lineation.

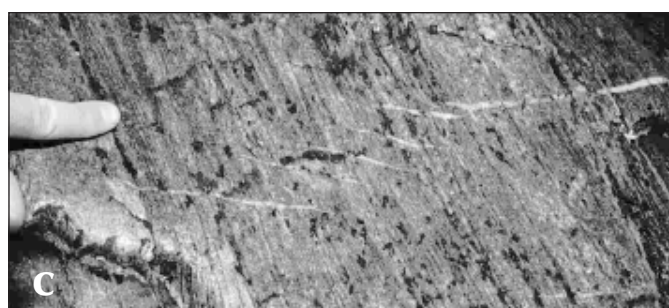
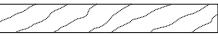
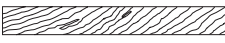





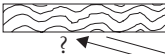
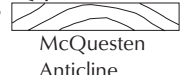


Figure 6. a) Boudin-neck quartz vein (DV_b). b) Tension veins (DV_c) in quartzite cutting earlier folded quartz vein (DV_a). c) Tension vein array (DV_c) in gritty quartzite.

Table 1. Paragenetic table of all ductile deformation features in the Clear Creek area. An attempt to correlate deformations defined by Murphy (1997) and Mair (this volume) is also made.

Deformations →	D ₁	D ₂	D ₃	D ₄	D ₅				
This study Clear Creek	 S ₁ spaced cleavage	 S ₂ schistosity, isoclinal F ₂ folds, peak regional metamorphism, boudinage	 S ₃ axial planar foliation, F ₃ folds, L ₃ extension lineation, boudinage	 Dv _a pervasive, isoclinally folded, boudinaged quartz veins	 Dv _b boudin-neck quartz veins	 Dv _c tension veins, TVAs	 Dv _d ~140° slightly boudinaged quartz veins	 F ₄ open crenulations	 McQuesten Anticline
Murphy et al., (1997) Entire THSZ		Sp, Sp' Lp?	Fc Lp?, Lpxc	Fc+?	McQuesten Anticline				
Mair et al., (this volume) Scheelite Dome		D ₁	D ₂						

BRITTLE DEFORMATION FEATURES

Brittle deformation in the area is manifest as three major fault/fracture sets, with corresponding veins, joints, aplite, granitoid and lamprophyre dykes. These structures post-date the ductile fabrics developed in the THSZ. The following kilometre-scale brittle structures were identified from mapping and air photo interpretation (Fig. 7):

- BF_a** South- to south-southeast-striking (~165°), steep, major faults with mostly apparent sinistral displacement (pre-, syn- and post-TPS emplacement; Fig. 7g).
- BF_b** East-southeast-striking (~115°), steep fracture zones (pre-, syn- and post-TPS emplacement; Fig. 7g)
- BF_c** Northeast-striking (~035°), steep fracture zones (uncertain of relative timing; Fig. 7g).

The dominant outcrop-scale brittle structures are correlated with the air photo-interpreted structures (equivalent subscripts) as follows:

- BV_a** South- to south-southeast-striking, steeply dipping quartz-tourmaline veins, aplite and granitoid veins/dykelets and joints (syn/post-TPS emplacement; Figs. 7a-f).
- BV_b** A dominant set of east- to east-southeast-striking (~115°), sheeted gold-bearing quartz veins, quartz-biotite veins, lamprophyre dykes and minor quartz-tourmaline veins. A subset of east-northeast-striking (~070°) aplite and quartz-tourmaline veins also occurs (late syn/post-TPS emplacement; Figs. 7a-f).
- BV_c** North-northeast-striking (~015°), minor set of quartz veins and joints (uncertain of relative timing; Figs. 7a-f).

BRITTLE GEOMETRICAL ANALYSIS

Stereonets and rose diagrams of brittle structural data (Fig. 7) collected at Clear Creek show the following features (all data in strike direction):

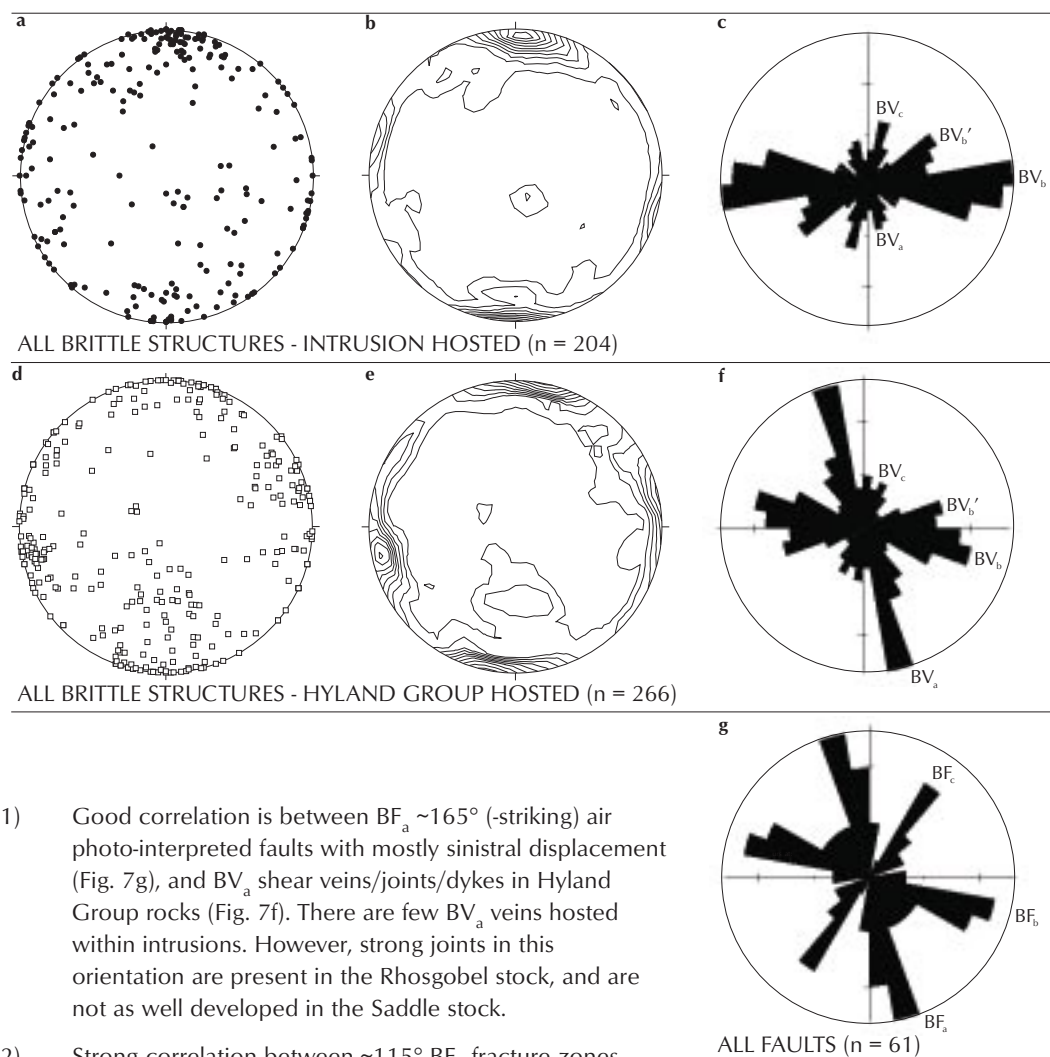


Figure 7. Stereonets and rose diagrams – all brittle structures measured in outcrop (a-f) and from air photo interpretation (g).

- 1) Good correlation is between BF_a ~165° (-striking) air photo-interpreted faults with mostly sinistral displacement (Fig. 7g), and BV_a shear veins/joints/dykes in Hyland Group rocks (Fig. 7f). There are few BV_a veins hosted within intrusions. However, strong joints in this orientation are present in the Rhosgobel stock, and are not as well developed in the Saddle stock.
- 2) Strong correlation between ~115° BF_b fracture zones (Fig. 7g) and BV_b tensile veins (Fig. 7f) in Hyland Group rocks. There is moderately good correlation with BV_b in intrusions (Fig. 7c), although the maxima is at ~085°. Possible subsets or conjugate sets of BV_b (BV_b') occur at ~055° within intrusions (Fig. 7c) and at ~075° in Hyland Group rocks (Fig. 7f).
- 3) Weak correlation is shown between ~035° BF_c air photo linears (Fig. 7g) and BV_c ~015° outcrop-scale structures (Fig. 7c, f).
- 4) Moderate similarity in orientation is displayed by the BV_c ~015° veins in both intrusions and Hyland Group rocks (Fig. 7c, f).

Therefore, in general, the km-scale faults and fractures correspond well with those at outcrop scale. The main differences include orientation of the tensile veins in Hyland Group rocks BV_b (~115°) versus those hosted in intrusions (maxima ~085°). In addition, the lack of dilatant ~165° structures measured within intrusions as compared to Hyland Group rocks is significant.

PRELIMINARY FAULT AND FRACTURE CONNECTIVITY ANALYSIS

Oliver (1999) stated, "In complex brittle settings, the relationship of individual fault branches or segments to the inferred far-field stresses is most important. The key structural condition for ore formation in any fault-related mineralized region is the linking up of fracture networks. In this case, relatively connected faults will form long-distance fluid channelways. Ore deposition may occur at specific structural sites such as terminal fault branches, faults in particular orientations, and smaller faults that connect larger faults."

Linked fault systems provide real-rock permeability and thus potential for major ore accumulation. However, real-time (syn-faulting) connectivity between faults is difficult to prove from field relations. Despite these difficulties, it is possible to make preliminary estimates of the degree of fault interconnectivity on a complex fracture array. A favourably oriented fault segment

that is linked to other faults is more likely to be able to transmit fluid considerable distance than one that is isolated in three dimensions (Oliver, 1999).

The Clear Creek area is dominated by three kilometre-scale brittle structural trends. Field mapping and air photo interpretation data indicate the BF_a/BV_a structures are mostly

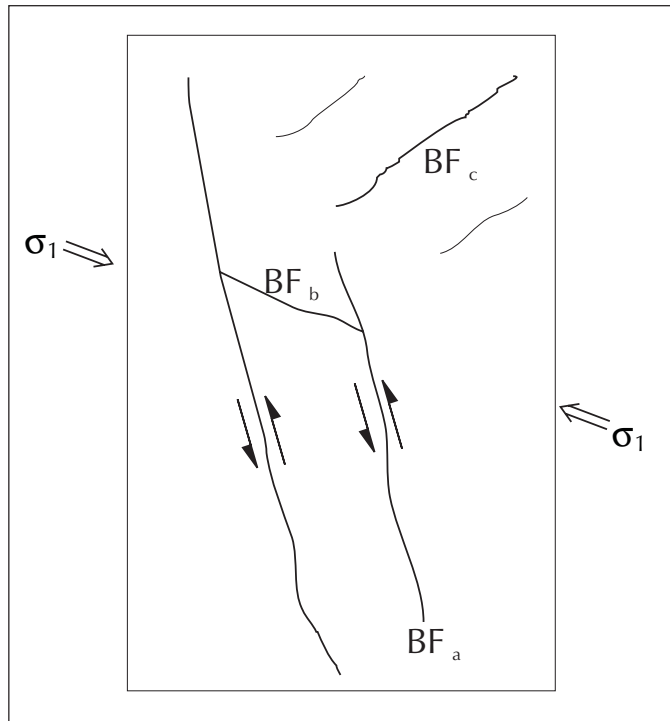


Figure 8. Schematic sketch of the major fault/fracture types at Clear Creek. BF_a are strike-slip faults, BF_b are transtensional and BF_c are transpressional faults.

sinistral faults and shear veins, BF_b/BV_b structures are mostly dilatant faults/fracture zones and tensile veins and dykes, and BF_c/BV_c structures are mostly antidilatational faults/fractures and joints. An interpretation of near east-west overall shortening in the area is permitted, where BF_a are strike-slip faults, BF_b are transtensional faults and BF_c are transpressional faults (Fig. 8).

These data suggest BF_a structures act as master faults, with BF_b and BF_c structures occurring as secondary fractures. Thus BF_a faults seem most likely to be able to transmit fluid over large distances. Straight sections of these faults, however, would not be particularly favourable sites for mineralization as they will not be very dilatant. More easterly striking, misoriented segments of these faults would be more dilatational and thus more favourable sites for mineralization (Fig. 9a). North-south oriented portions of these faults, that is $\sim 180^\circ$ striking, will be antidilatational and thus poor targets for mineralization (Fig. 9b). BF_b structures are by far the most dilatational set in the area. Therefore any BF_b structure directly connected to a BF_a fault conduit could provide an ideal site for fluid trapping and thus mineralization (Fig. 9c). Furthermore, any BF_b structure linking two BF_a faults should be very highly regarded as an exploration target (Fig. 9d). BF_c structures seem to be the least dilatational of the three sets, and thus are considered poor targets for mineralization. It should be noted, however, that a reversal in the shear-sense on BF_a faults could make BF_c structures dilatational (Fig. 9e).

MINERALIZATION

A number of styles of gold mineralization are present at Clear Creek, with accompanying tungsten and silver-lead. Marsh et al. (1998) identified two geochemically distinct metal suites in the Clear Creek gold occurrences. The first is characterized by As-Au-Bi \pm Sb and Te association, with a minor metal factor defined

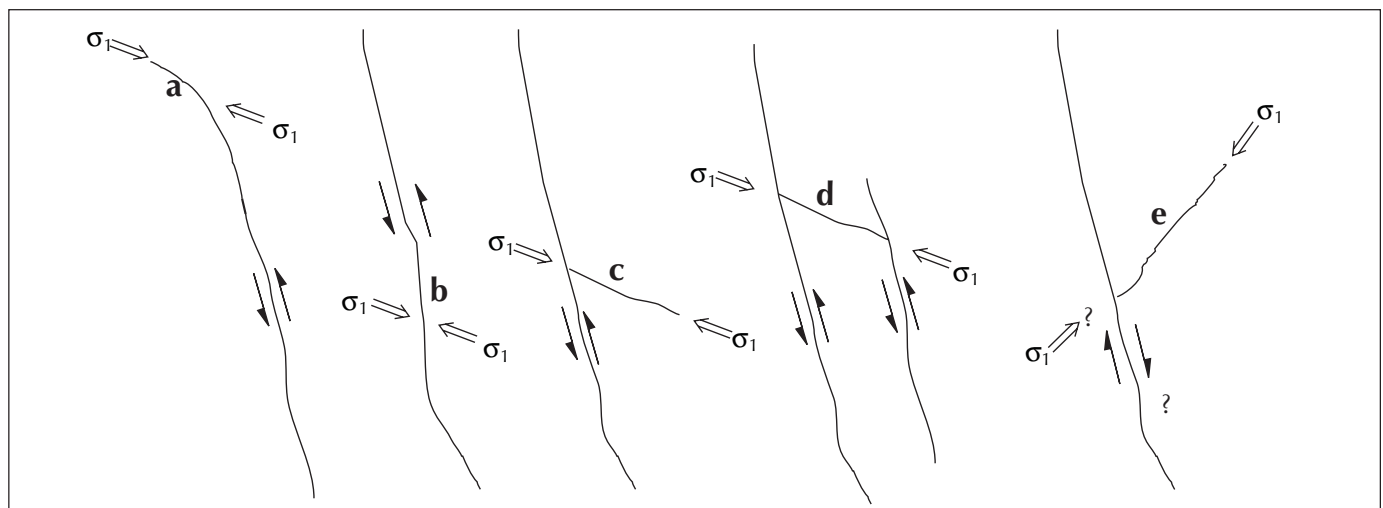


Figure 9. Favourable structural sites for mineralization a) favourably misoriented segment of BF_a fault b) unfavourably misoriented segment of BF_a fault c) BF_b fracture zone linked to BF_a fault d) BF_b fracture zone linking two BF_a faults e) BF_c fracture zone connected to BF_a fault, perhaps with dextral movement.

Table 2. Paragenetic table depicting the geological history during brittle deformation. Note the timing of BF_c/BV_c structures is uncertain.

KEY TIMING → CONSTRAINTS	TPS EMPLACEMENT	E-W Au-BEARING QUARTZ VEINS	~165° QUARTZ-TOURMALINE SHEAR VEINS
Bf_a	fracturing faulting jointing	regional fractures becoming ~165° oriented faults	sinistral reactivation on ~165° faults
Bv_a	granitoid sills and dykes aplite dykelets and veins		quartz tourmaline sinistral shear-veins
Bf_b	in Hyland Group in TPS intrusions		
Bv_b	granitoid sills and dykes aplite dykelets and veins (070° subset) tourmaline-bearing pegmatites tourmaline-bearing quartz-veins (070° subset) biotite quartz veins (reactive selvage) aplitic molybdenite-bearing veins	~105° gold-bearing quartz sulphide veins in Hyland Group ~085° gold-bearing quartz sulphide veins in TPS intrusions lamprophyre dykes	
Bf_c Bv_c	fracture zones associated with possible dextral movement on Bf_a faults	OR minor quartz sulphide veins	
	91.4 ± 0.8 Ma contact metamorphism associated with TPS pervasive H_2O_2 rich fluids	TPS intrusion structurally controlled fluid-flow vein dominant	TPS-related fluids

by Ag-Bi-Pb ± As, Au and Te. Tungsten was more erratic, and showed no particular association with either of the above metal factors.

Mineralization styles identified in this study are outlined by previous workers (e.g., Emond and Lynch, 1990; Marsh et al., 1999; Murphy, 1997) and others. These are correlated within the proposed structural framework as follows and in Table 2 (locations of stocks and zones in Figure 2).

- East-west sheeted quartz veins within intrusions, e.g., Rhosgobel stock (BF_b/BV_b zone connected to BF_a fault), Eiger stock (BV_b zone connected to misoriented section of BF_a fault).
- East-west sheeted quartz veins in Hyland Group, e.g., Josephine Switchback (BV_b).
- Silicified shear-zones, e.g., Contact Zone ($BF_b?$).
- Distal or roof-zone fault breccias, e.g., Bear Paw breccia (misoriented segment of BF_a fault?).

- Aplitic-molybdenite-bearing veins, e.g., Harper Creek (BV_b).
- Distal silver-lead fault breccia zones, e.g., Galena Zone (BF_b/BF_c intersection, linked to BF_a fault).
- Scheelite-bearing quartz veins in calc-silicate rocks and skarns, e.g., Harper Creek (BV_b).
- Arsenopyrite alteration of diopside in alteration selvages of deformed DV_a/DV_b quartz veins, e.g., Harper Creek (overprinting of DV_a and DV_b veins during contact metamorphism/metasomatism).
- Disseminated arsenopyrite associated with metasomatism of calc-silicate rocks, e.g., Harper Creek (pervasive fluid-flow controlled by pre-existing S_2 and S_3 fabrics).

The main mineralization styles therefore support the fault connectivity model proposed above which predicts BF_b structures and misoriented BF_a faults will be the most dilational and thus most favourable sites for mineralization.

PARAGENESIS AND STRUCTURAL EVOLUTION

The overall paragenesis from ductile deformation/regional metamorphism through to granite emplacement, contact metamorphism and related veining and mineralization (Figs. 10-12) can be used in a preliminary attempt to model the changing stress field over time.

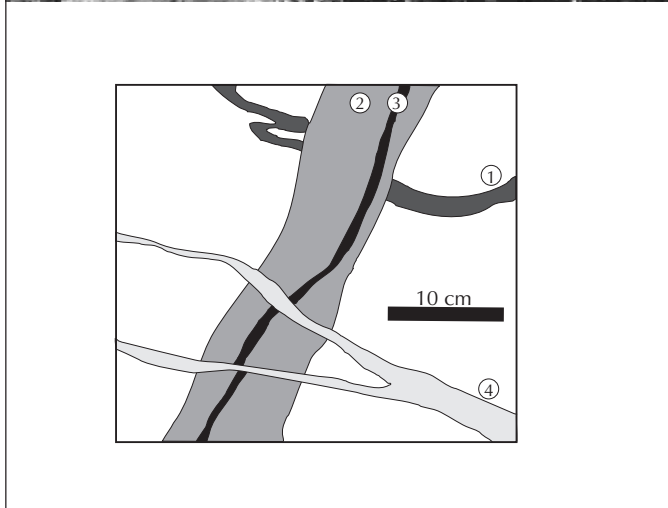
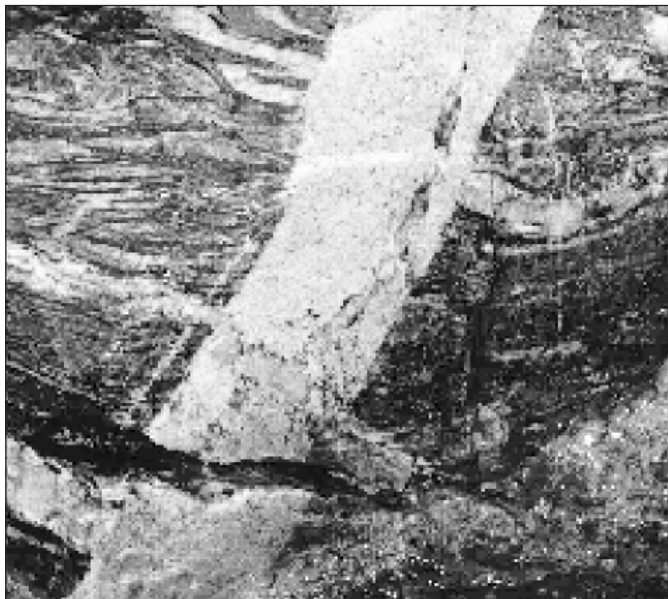


Figure 10. THSZ-related, isoclinally folded quartz vein 1 (DV_a) cut by aplite dykelet 2 (BV_a), which is in turn cut by a quartz-tourmaline vein 3 (BV_a). Finally, all features are cut by moderately north-dipping quartz veins 4 (BV_b - gold mineralized set).

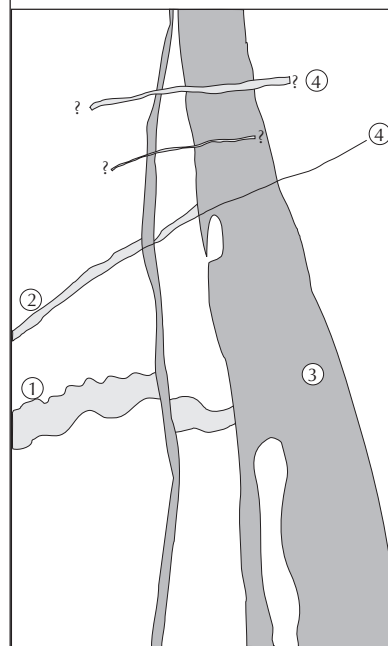


Figure 11. THSZ-related boudin-neck quartz vein 1 (DV_b), and $\sim 140^\circ$ oriented, slightly boudinaged quartz vein 2 (DV_d) cut by quartz-monzonite dykelets 3 (BV_b). Late quartz \pm tourmaline veins 4 (BV_a) cut the monzogranite, and a joint propagates along 2.

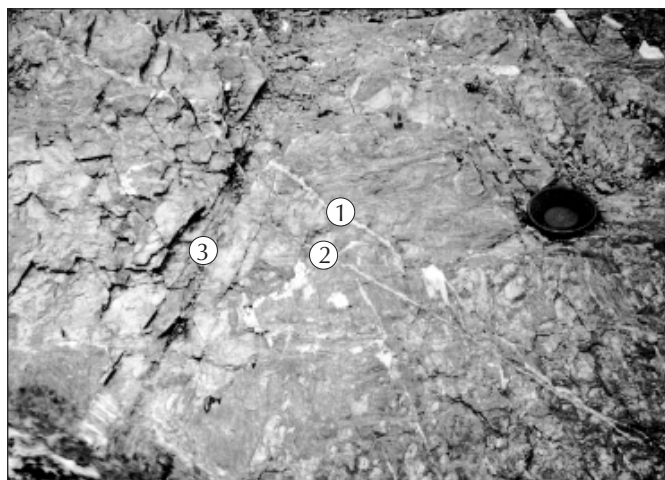


Figure 12. Slightly wavy, aplitic quartz vein 1 (BV_b) cut by sheeted quartz vein 2 (BV_b). A quartz-tourmaline sinistral shear vein 3 (BV_a) cuts both 1 and 2.

One possible model for the development of the brittle structural architecture at Clear Creek is proposed in Figure 13.

- a) Northwest-southeast directed σ_1 probably initiated $\sim 165^\circ$ striking faults (BF_a) with sinistral movement (Fig. 13a).
- b) The BF_b and BV_b tensile fracture/vein set was probably initiated within Hyland Group rocks by a slight ($\sim 30^\circ$) anticlockwise rotation of σ_1 . This set has formed broadly en echelon to the sinistral $\sim 165^\circ$ oriented faults (BF_a ; Fig. 13b).
- c) Emplacement of the TPS then occurred, with possible pre-existing control by $\sim 165^\circ$ faults (BF_a , e.g., Saddle and Rhosgobel stocks) and some east-west control (e.g., Barney and Grizzly stocks), also reflected regionally in the TPS (Fig. 13c).
- d) Further development of BF_b and BV_b structures occurred, particularly within intrusions that had crystallized and cooled, with σ_1 possibly further rotated to the east-west. This rotation is reflected in the dominant $\sim 085^\circ$ orientation of BV_b veins within the intrusions. At this stage, $\sim 165^\circ$ BF_a faults would lock up due to their high angle with σ_1 , and BF_b/BV_b could take up most of the strain by north-south extension and thus dilation (Fig. 13d).

take up most of the strain by north-south extension and thus dilation (Fig. 13d).

- e) The final stage of deformation was sinistral reactivation on $\sim 165^\circ$ BF_a faults with associated development of quartz-tourmaline shear veins that cut all ductile and brittle features (Fig. 13e).

There are a number of problems with the above model which are detailed as follows:

- The timing of BF_c/BV_c structures in the area remains unresolved.

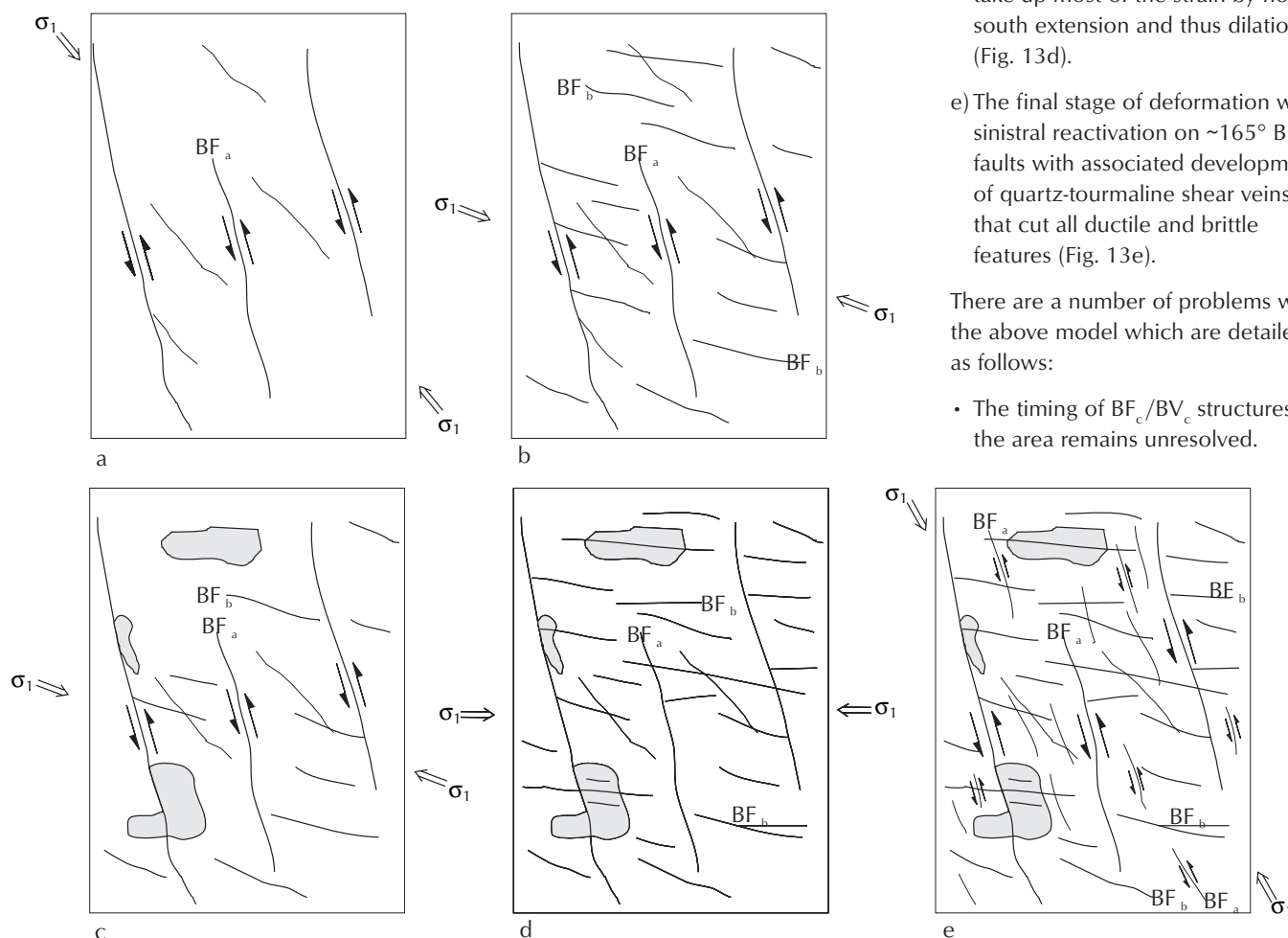


Figure 13. Preliminary model for the structural evolution at Clear Creek (see text).

- The model does not explain possible $\sim 055^\circ$ and $\sim 075^\circ$ striking subsets/conjugates of the BV_b vein set.
- The difference in BV_b orientations between Hyland Group rocks and TPS intrusions could be explained by refraction through the more brittle plutons.
- Real fault solutions could not be determined due to a lack of markers in the strongly deformed Hyland Group. Fault movements were mainly assumed from stepped slickensides, angular relationships and foliation surfaces bending into faults.
- The timing of large-scale structures in the area is equivocal from aerial photography; thus relationships on outcrop-scale that have been applied to these structures may lead to potential mis-correlation.

On a broader scale, a number of features indicate the possibility of a crustal-scale controlling structure for the TPS belt and related mineralization. These include the broad east-west orientation of the TPS belt, east-west dominant sheeted veins and east-west oriented lamprophyre dykes. These data, in addition to local structural data suggest the possibility of a Riedel shear model (Fig. 14). The east-west oriented TPS belt could be the upper crustal manifestation of a *master fault (C)*, with *low angle Riedel (R)* and *high angle Riedel (R')* shears represented by BF_b/BV_b and BF_a/BV_a structures, respectively. The *pressure shears (P)* may be represented by the subset BV_b' structures.

DISCUSSION

It is apparent that the rocks in the Clear Creek area have undergone a protracted history involving ductile, brittle-ductile and brittle deformation. The intense ductile deformation history has been overprinted by the later contact metamorphism, metasomatism and brittle deformation associated with TPS intrusions. An extensive system of buried TPS intrusions is indicated by very broad contact metamorphic aureoles at Clear Creek.

Application of basic fault percolation analysis suggests the most favourable sites for fluid pooling, and thus gold mineralization, are BF_b fracture zones connected to BF_a fault conduits (Fig. 13). Any BF_b fracture zones linking two BF_a faults should be even more highly regarded. Misoriented, more easterly striking segments of BF_a faults should also be considered as exploration targets. The timing of BF_c northeast-oriented fracture zones is not known, however any of these linked to major BF_a faults could provide dilational sites for mineralization.

TPS intrusions are widely considered the source of mineralizing fluids (Thompson et al., 1999); thus proximity to these intrusions is considered to be a major factor controlling the occurrence of gold mineralization. The recently discovered Bear Paw breccia zone is likely to be located above buried intrusions, and may represent a new roof-zone style of mineralization. This structural exploration model therefore ranks highly those favourable structural sites that

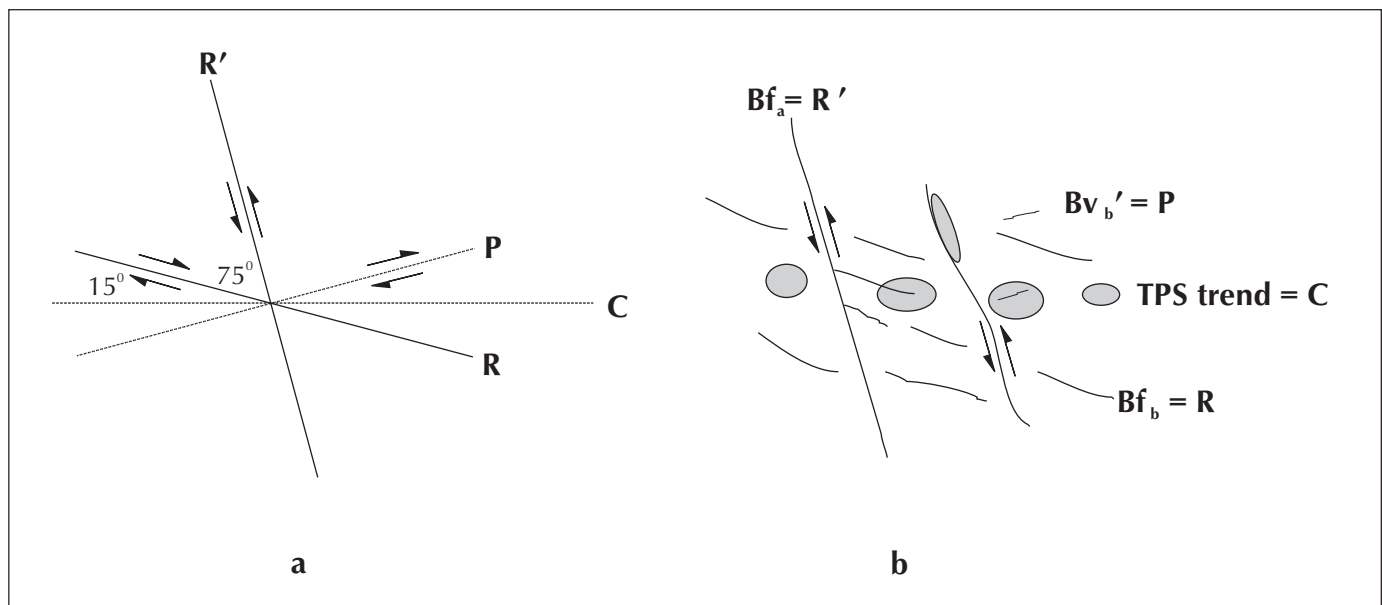


Figure 14. Possible application of a Riedel shear model to the Clear Creek area. *C* is represented by the E-W trend of the TPS belt, *R'* is represented by BF_a sinistral faults, *R* is represented by BF_b/BV_b fracture zones and veins, *P* is represented by the subset BV_b' (only observed at outcrop scale).

are coincident with shallowly buried TPS intrusions, or associated with ~165° BF_a faults that link into TPS intrusion systems.

Other TPS intrusion-related gold mineralization and deposits within the Selwyn Basin have similar dominant brittle structural trends to Clear Creek (e.g., Brewery Creek: Lindsay, this volume; Scheelite Dome: Mair, this volume). This, in addition to the coincident broad east-west trend of the TPS belt, dominant east-west sheeted veins and lamprophyre dykes suggests a crustal-scale controlling structure at depth such as a basement block boundary or a former suture zone. A Riedel shear model (Riedel, 1929) is therefore possible and is not mutually exclusive of the structural evolution proposed above.

FURTHER WORK

Continuing work on the structural, thermal and chemical evolution of TPS-related gold deposits will include:

- 1) Detailed petrography, fluid inclusion, stable isotope and Ar-Ar dating on collected samples to further constrain the paragenetic sequence of events defined in the field. A particular emphasis will be placed on constraining pressures of TPS emplacement and mineralization.
- 2) Similar work to be undertaken at Dublin Gulch should provide a framework for a regional-scale fault and fracture analysis. This will involve comparisons with other TPS-related deposits (e.g., Scheelite Dome and Brewery Creek), and mechanical modelling of fault/fracture arrays.
- 3) Petrologic and hydrothermal geochemical modelling of contact aureole fluid/rock interaction may constrain fluid-flow paths and fluxes around TPS intrusions.
- 4) Structural mapping of ca. 65 Ma McQuesten suite intrusions west of Clear Creek may provide links to the deformation regime associated with TPS intrusions. The longevity of any crustal-scale structures would be of particular interest.

ACKNOWLEDGEMENTS

Thanks to everyone at the YGP for their help, in particular Lisabeth Bryon, Kaori Torigai, Melanie Reinecke and Leyla Weston. Discussions with Don Murphy, Richard Goldfarb and Don Keedicks were very helpful. Nels, Madeline and Dianne Harper provided excellent accommodation and entertainment at Clear Creek. Erin and Aladdin Marsh and John Mair are thanked for their help in the field and interesting discussions. Thanks also to Mike Stammers from Pamicon and Redstar Resources for useful discussions and providing some transportation while in the field.

REFERENCES

- Allen, T.L., Hart, C.J.R and Marsh, E.E., 1999. Placer gold and associated heavy minerals of the Clear Creek drainage, central Yukon: Past to present. *In: Yukon Exploration and Geology 1998*, C.F. Roots and D.S. Emond (eds.), Exploration and Geological Services Division, Yukon, Indian and Northern Affairs Canada, p. 197-214.
- Baker, T. and Lang, J.R., 1999. Geochemistry of hydrothermal fluids associated with intrusion hosted gold mineralization, Yukon Territory. *In: Mineral Deposits: Processes to Processing*, Stanley et al., (eds.), Balkema, Rotterdam, p. 17-19.
- Emond, D.S. and Lynch, T., 1990. Geology, mineralogy and geochemistry of tin and tungsten veins, breccias and skarns, McQuesten River region (115P (north) and 105M 13), Yukon. *In: Yukon Geology, Volume 3*, Exploration and Geological Services Division, Yukon, Indian and Northern Affairs Canada, p. 133-159.
- Lindsay, M.J., Baker, T., Oliver, N.H.S., Diment, R. and Hart, C.J.R., 2000 (this volume). The magmatic and structural setting of the Brewery Creek gold mine, central Yukon. *In: Yukon Exploration and Geology 1999*, D.S. Emond and L.H. Weston (eds.), Exploration and Geological Services Division, Yukon, Indian and Northern Affairs Canada, p. 219-227.
- Mair, J.L., Hart, C.J.R, Goldfarb, R. J., O'Dea, M. and Harris, S., 2000 (this volume). Geology and metallogenic signature of gold occurrences at Scheelite Dome, Tombstone gold belt, Yukon Territory. *In: Yukon Exploration and Geology 1999*, D.S. Emond and L.H. Weston (eds.), Exploration and Geological Services Division, Yukon, Indian and Northern Affairs Canada, p. 165-176
- Marsh, E.E., Hart, C.J.R, Goldfarb, R.J. and Allen, T.L., 1999. Geology and geochemistry of the Clear Creek gold occurrences, Tombstone gold belt, central Yukon Territory. *In: Yukon Exploration and Geology 1998*, C.F. Roots and D.S. Emond (eds.), Exploration and Geological Services Division, Yukon, Indian and Northern Affairs Canada, p. 185-196.
- Murphy, D.C., 1997. Geology of the McQuesten River region, northern McQuesten and Mayo map areas, Yukon Territory (115P/14, 15, 16; 105M/13, 14). Exploration and Geological Services Division, Yukon, Indian and Northern Affairs Canada, Bulletin 6, 122 p.
- Oliver, N.H.S., 1999. Analysis and mechanics of fractures, faults & veins: Application to fluid flow and mineralization. Short-course notes, Economic Geology Research Unit, School of Earth Sciences, James Cook University, Queensland, Australia, 29 p.
- Riedel, W., 1929. Zur Mechanik geologischer Brucherscheinungen. *Cbl.f.Min., Abt. B.*, p. 354-368.
- Thompson, J.H.F., Sillitoe, R.H., Baker, T., Lang, J.R. and Mortenson, J. K., 1999. Intrusion-related gold deposits associated with tungsten-tin provinces. *Mineralium Deposita*, vol. 34, p. 323-334.

